Experimental investigation of shell-model excitations of ^{89}Zr up to high spin

S. Saha,[1] R. Palit,[1,*] J. Sethi,[1] T. Trivedi,[1] P. C. Srivastava,[2] S. Kumar,[3] B. S. Naidu,[1] R. Donthi,[1] S. Jadhav,[1] D. C. Biswas,[4] U. Garg,[5] A. Goswami,[6] H. C. Jain,[1] P. K. Joshi,[1,†] G. Mukherjee,[7] Z. Naik,[8] S. Nag,[9] V. Nanal,[1] R. G. Pillay,[1] S. Saha,[6] and A. K. Singh[9]

[1]*Department of Nuclear and Atomic Physics, Tata Institute of Fundamental Research, Mumbai 400005, India*
[2]*Instituto de Ciencias Nucleares, Universidad Nacional Autónoma de México, 04510 México, Distrito Federal, Mexico*
[3]*Department of Physics and Astrophysics, University of Delhi, Delhi 110007, India*
[4]*Nuclear Physics Division, Bhabha Atomic Research Centre, Mumbai 400085, India*
[5]*Physics Department, University of Notre Dame, Notre Dame, Indiana 46556, USA*
[6]*Saha Institute of Nuclear Physics, Kolkata 700064, India*
[7]*Variable Energy Cyclotron Centre, 1/AF, Bidhan Nagar, Kolkata 700064, India*
[8]*Physics Department, Sambalpur University, Sambalpur 768019, India*
[9]*Department of Physics & Meteorology, Indian Institute of Technology, Kharagpur 721302, India*

(Received 2 August 2012; revised manuscript received 27 August 2012; published 10 September 2012)

Near yrast states in ^{89}Zr were investigated up to high spin using the fusion evaporation reaction ^{80}Se(^{13}C, $4n$) at an incident beam energy of 50 MeV. Excited levels of ^{89}Zr have been observed up to ∼10 MeV excitation energy and spin $\sim 37/2\hbar$ using the prompt gamma spectroscopy technique with the Indian National Gamma Array (INGA). The angular distribution, directional correlation, and polarization measurements were carried out to assign the spin and parity of the newly reported states. The structures of both the positive and negative parity states up to highest spin observed in the present experiment have been compared with shell-model calculations using two recently developed residual interactions, JUN45 and jj44b. The role of proton excitations from $p_{3/2}$ and $f_{5/2}$ orbitals to the $g_{9/2}$ orbital for the higher spin states has been discussed.

DOI: 10.1103/PhysRevC.86.034315 PACS number(s): 23.20.En, 23.20.Lv, 27.50.+e, 29.30.Kv

I. INTRODUCTION

The excited states of nuclei near the $N = 50$ closed shell have attracted a lot of attention in theoretical and experimental research. They provide a suitable laboratory for testing the interactions of shell-model states and the possible presence of high spin isomers, and they help in understanding the shape transition as the higher j orbitals are occupied [1–6]. The occupation of shape-driving orbitals at higher spin gives rise to the emergence of regular band structure with increasing excitation energy. For nuclei with $N = 48$ to 50, there are four active neutron orbitals $p_{3/2}$, $f_{5/2}$, $p_{1/2}$, and $g_{9/2}$ which contribute to the level structure of these nuclei through the mixing of different configurations involved with these orbitals. In particular, the structure of $N = 49$ isotones (and $Z = 32$ to 46) with one hole in the $N = 50$ shell gap has been investigated using different reactions. While the lighter isotones such as ^{83}Se were investigated in fusion-fission experiments up to medium spin [7], the heavier isotones ^{91}Mo, ^{93}Ru, and ^{95}Pd were studied up to higher spin using fusion evaporation reactions [1,8,9]. The low-lying states up to moderate spin for these $N = 49$ isotones with changing proton number test the shell-model interactions with limited available configurations due to the single neutron hole. Interestingly, the high spin states in these isotones have contributions from particle excitations across the respective shell gaps and provide a suitable testing ground for the prediction of shell-model interactions describing these excitations. The nucleus ^{89}Zr, having $Z = 40$ subshell closure and one neutron hole below the $N = 50$ shell gap, is a good candidate to investigate the role of proton excitations across the $Z = 40$ subshell gap in explaining the high spin states. Extensive studies of the high spin states of heavier $N = 49$ isotones starting with ^{91}Mo up to ^{95}Pd are available. However, limited information exists on the high spin states of lighter isotones in the literature. Therefore, the motivation of the present work is to extend the high spin structure of ^{89}Zr and to characterize the structure of these levels through comparison with large-scale shell-model calculations. In the present work, we will discuss the spectroscopic study of the high spin states of the ^{89}Zr isotope.

The knowledge of high spin states in ^{89}Zr was very limited prior to the present work. The high spin states of ^{89}Zr have been studied using the ^{88}Sr(α,$3n$)^{89}Zr, ^{76}Ge(^{18}O,$5n$)^{89}Zr, and ^{74}Ge(^{18}O,$3n$)^{89}Zr reactions with smaller arrays with up to three high-purity germanium (HPGe) detectors [10,11]. Levels of ^{89}Zr have also been studied using (p, t), (p, d), (d, t), $(p, n\gamma)$, and (^{3}He,α) reactions [12–15] apart from radioactive decay investigations [16].

For nuclei in this region many shell-model calculations have been performed, using different model spaces as well as different interactions, in order to describe the overall properties as a function of the mass, or specific key nuclei [2,3,17–19]. An elaborate shell-model calculation in the mass range $A = 86$–100 for the isotopes near the proton drip line was performed by Herndl and Brown [3] to calculate binding energies and beta-decay half-lives as input for astrophysical processes. The role of the intruder $g_{9/2}$ orbital, the possible proton closure at

*Corresponding author: palit@tifr.res.in
†Present address: Homi Bhabha Centre for Science Education, TIFR, Mumbai 400088, India.

$Z = 38$ or 40, and the spherical-deformed phase transition were extensively discussed in these calculations. The model space consisting of only the upper two orbits $p_{1/2}$ and $g_{9/2}$ has been frequently adopted for the description of nuclei around $N \sim 50$ and $Z \sim 40$ [3,18,20]. Recently, a new effective interaction for shell-model calculations in the model space consisting of $1p_{3/2}$, $0f_{5/2}$, $1p_{1/2}$, and $0g_{9/2}$ spherical orbits (referred to as f_5pg_9 shell space hereafter) has been presented, and as one of its applications the systematic studies of $N = 49$ odd-odd isotopes were discussed [21]. Similarly, the jj44b interaction by Brown *et al.* [22] was developed by fitting 600 binding energies and excitation energies with $Z = 28$–30 and $N = 48$–50. The results of the shell-model calculations based on these two interactions have been also compared with the measured spin and moments of the various isotopes of Ga, Sr, and Zr in Refs. [23,24]. It will be interesting to discuss the measured high spin states of ^{89}Zr in our experiment with the results of these new interactions to investigate the predictive power of the shell-model.

We have organized the paper in five sections. In Sec. II, the experimental setup and the data analysis procedure are discussed. The experimental results and the ^{89}Zr level scheme are presented in Sec. III. The results are discussed within the framework of the shell model in Sec IV. Finally, a brief summary of the present work is given in Sec. V.

II. EXPERIMENTAL DETAILS AND ANALYSIS PROCEDURE

Excited states of ^{89}Zr were produced in the in-beam experiment using the ^{13}C + ^{80}Se reaction at 50 MeV beam energy. The ^{13}C beam was provided by the Pelletron Linac facility at Mumbai. The target consisted of 800 μg/cm^2 ^{80}Se evaporated on Au backing with a thickness of 9 mg/cm^2 in the experiment. The Indian National Gamma Array (INGA) consisting of eighteen Compton- suppressed clover detectors was used to detect the γ rays emitted in the reaction. In the present configuration of the INGA, the Compton-suppressed clover detectors were arranged in the rings at 40°, 65°, 90°, 115°, 140°, and 157° with respect to the beam direction [25]. Two- and higher-fold clover coincidence events were recorded in a fast digital data acquisition (DDAQ) system based on Pixie-16 modules of XIA LLC [26,27]. In addition, for the measurement of the angular distribution of the γ rays the DDAQ was also used in singles mode. ^{133}Ba and ^{152}Eu radioactive sources were used for the energy calibration and determination of relative photopeak efficiency of the array. Data from radioactive decay of ^{66}Ga ($T_{1/2} = 9.41$ h) has been used [28] for the determination of the photopeak efficiency of γ rays with energy higher than 1500 keV.

The data sorting routine "MultipARameter time-stamp-based COincidence Search program (MARCOS)," developed at the Tata Institute of Fundamental Research (TIFR), sorts the time-stamped data to generate one-dimensional histograms, E_γ-E_γ matrices, and E_γ-E_γ-E_γ cubes. The time window for the prompt $\gamma\gamma$ coincidence was set to 150 ns. The RADWARE software package [29] was used for the analysis of these matrices and cubes. Each of the clover detectors was used in add-back mode, and the add-back data were used to construct these matrices and cubes for further analysis. Angle-dependent asymmetric E_γ-E_γ matrices were constructed for the measurements of the directional correlations and polarization asymmetry of the emitted γ rays, in order to assign the spin parity to the excited states. The energy, intensities, directional correlation of oriented states (DCO), and polarization measurements of the γ rays were carried out from the time-stamped data. A total of 1×10^9 coincidence events with fold $f \geqslant 2$ were collected during the experiment.

The partial level scheme of ^{89}Zr established in the present work is shown in Fig. 1. The total projection spectrum obtained from the matrix is given in Fig. 2 and shows the strong transitions from ^{88,89,90}Zr and ^{89}Y produced in the current reaction. Various gated spectra relevant for identifying transitions of the level scheme of ^{89}Zr are shown in Figs. 3–5.

The angular distributions for some of the strong transitions were measured to determine their multipolarities. The γ rays were detected in the singles mode by the clover detectors placed at angles of 157°, 140°, 115° and 90°, 65°, 40° with respect to the beam direction. The angular distribution plots for the 1944 and 781 keV transitions are shown in Fig. 6. The a_2 and a_4 coefficients for the angular distribution of these transitions suggest the pure $\Delta I = 2$ nature. These transitions were used for gating purpose in the extraction of directional correlation of oriented states (DCO) ratios for many of the newly identified transitions decaying from the higher excited states.

The directional correlation of oriented states (DCO) and integrated polarization direction correlation (IPDCO) analysis of different transitions were carried out to determine the spin and parity of excited states. The spin assignments of the various excited states reported in this paper were correlated with the generic assumption that, for the states populated in heavy-ion fusion evaporation reactions, an increase in excitation energy is usually correlated with increase in spin. The multipolarities of γ rays were deduced from the angular correlation analysis [30] using the DCO ratio method of two coincident γ rays, γ_1 and γ_2, given by

$$R_{DCO} = \frac{I(\gamma_1) \text{ observed at } 157^\circ \text{ gated on } \gamma_2 \text{ at } 90^\circ}{I(\gamma_1) \text{ observed at } 90^\circ \text{ gated on } \gamma_2 \text{ at } 157^\circ}. \quad (1)$$

Here, $I(\gamma_1)$ represents the intensity of γ_1 measured in coincidence with γ_2. In the present geometry of detectors, the DCO ratios obtained with a stretched quadrupole (dipole) gate are 0.5 (1.0) and 1.0 (2.0) for the pure dipole and quadrupole transitions, respectively. The extracted DCO values were obtained with gate on strong stretched $\Delta I = 2$ or $\Delta I = 1$ transitions (see Table I).

The DCO values of most of the transitions from the higher levels in the positive parity bands were obtained with gates either on 1944 or 781 keV transitions, both being stretched $\Delta I = 2$ transitions. Similarly, for the transitions of the lower negative parity states (up to the $25/2^-$ state with excitation energy of 5496 keV), the 1559 keV transition was used for gating purpose. The DCO ratio of 1559 keV transition obtained with the 1994 keV gate suggests its stretched $\Delta I = 2$ character.

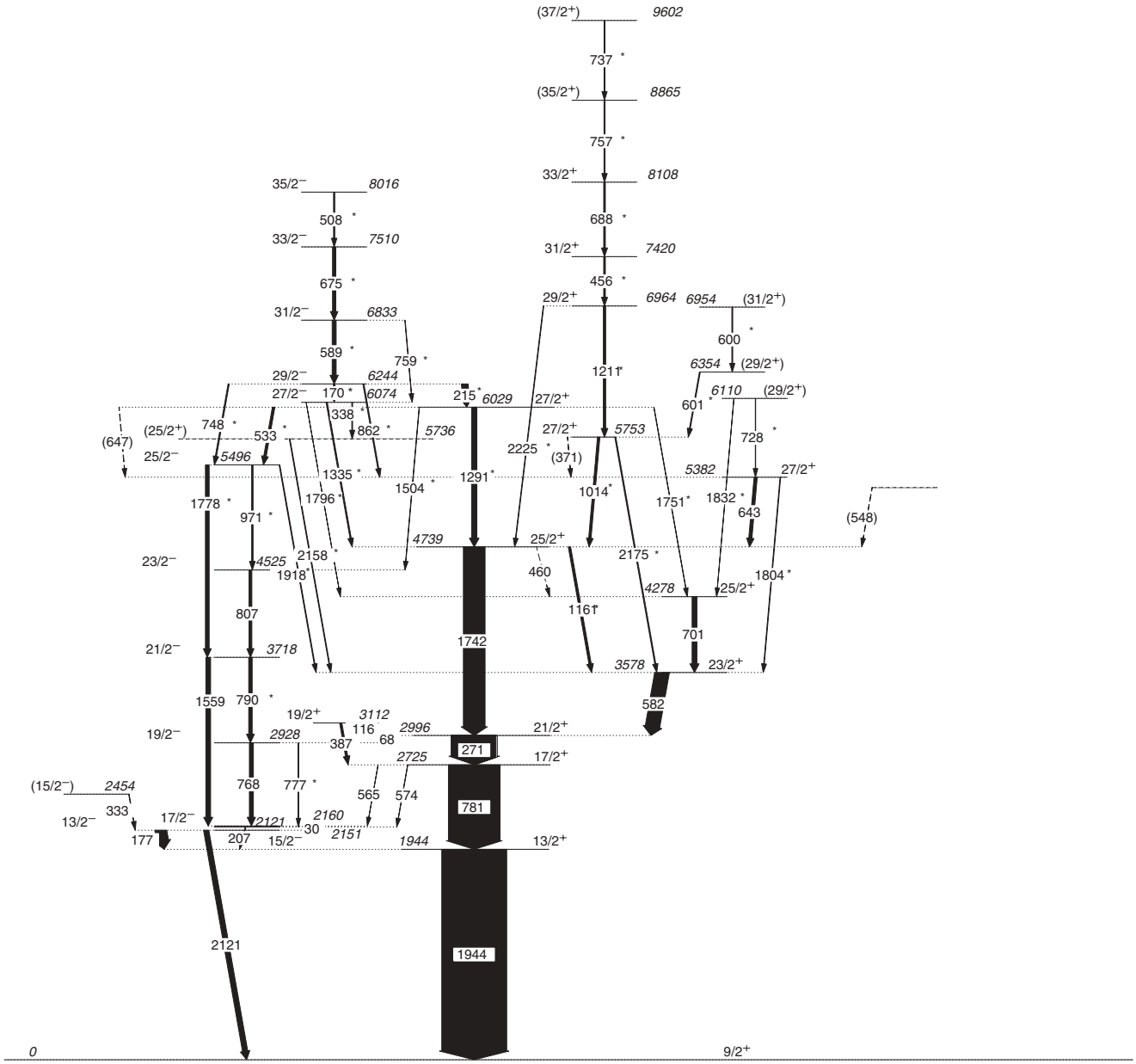

FIG. 1. Partial level scheme of ^{89}Zr deduced in the present work. The γ-ray energies are in keV. New transitions are indicated by asterisks.

Each of the four clover detectors present at 90° was used as a Compton polarimeter to assign the electric or magnetic nature of γ rays [31,32]. For a Compton polarimeter, polarization asymmetry Δ of the transition is defined as [31]

$$\Delta = \frac{a(E_\gamma)N_\perp - N_\parallel}{a(E_\gamma)N_\perp + N_\parallel}, \qquad (2)$$

where $N_\perp$ ($N_\parallel$) is the number of counts of γ transitions scattered perpendicular (parallel) to the reaction plane. The correction factor $a(E_\gamma)$ is a measure of the perpendicular-to-parallel scattering asymmetry within the crystals of the clover detector. For the 90° detectors this parameter has been found to be 1.00(1) from the analysis of decay data of the ^{133}Ba and ^{152}Eu radioactive sources. For linear polarization measurement, two asymmetric matrices corresponding to parallel and perpendicular segments of clover detectors (with respect to the emission plane) along one axis and the coincident γ rays from the other detectors along another axis were constructed [33]. Then integrated polarization direction correlation (IPDCO) analysis was carried out. A positive value of the IPDCO ratio indicates an electric transition, while a negative value indicates a magnetic transition. The positive and negative asymmetry parameters of different transitions depicted in Fig. 7 indicate their electric and magnetic nature, respectively. The 1559 keV gated spectra generated from parallel ($N_\parallel$) and perpendicular ($a(E_\gamma)N_\perp$) scattering events observed in the 90° clover detectors are shown in Fig. 8. Higher counts for 589 and 675 keV transitions in parallel scattered spectrum indicates their magnetic character while the reverse condition suggests the electric nature for the 533 keV transition. The

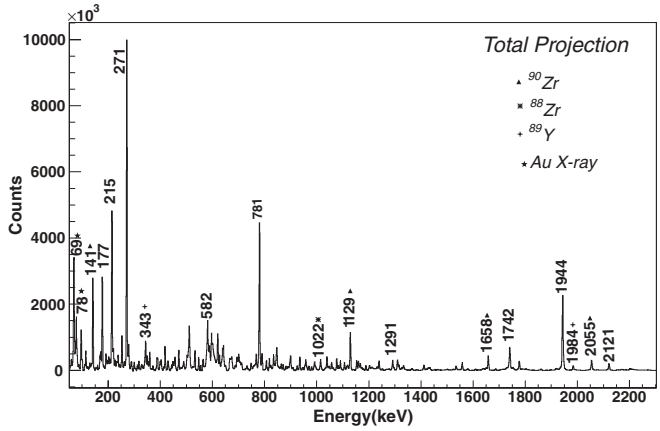

FIG. 2. The total projection spectrum depicting the strong transitions in keV which belong to ^{88,89,90}Zr and ^{89}Y isotopes produced in the current reaction $^{13}C + ^{80}Se$ at 50 MeV beam energy. The strong transitions of ^{88}Zr, ^{90}Zr, and ^{89}Y are marked by solid triangles, stars, and plus signs, respectively. The rest of the peaks labeled with their energy in keV are associated with ^{89}Zr, and indicate its highest yield in the present reaction.

inset spectrum confirms the electric and magnetic nature of the previously known 1944 and 2121 keV transitions, respectively.

The intensities, DCO, and polarization measurements of the different transitions are presented in Table I.

III. RESULTS

Prompt $\gamma\gamma$ coincidence analysis was performed to construct the level scheme of ^{89}Zr. The gate width of the prompt timing was set to 150 ns. The previous level scheme of ^{89}Zr was studied up to the $27/2^+$ state at 5.3 MeV excitation energy [10]. By gating on the known γ rays of the previous level scheme, about 35 new γ rays were assigned to ^{89}Zr. The new transitions are indicated by asterisks in the level scheme Fig. 1. The excitation energies of different levels and the ordering of the

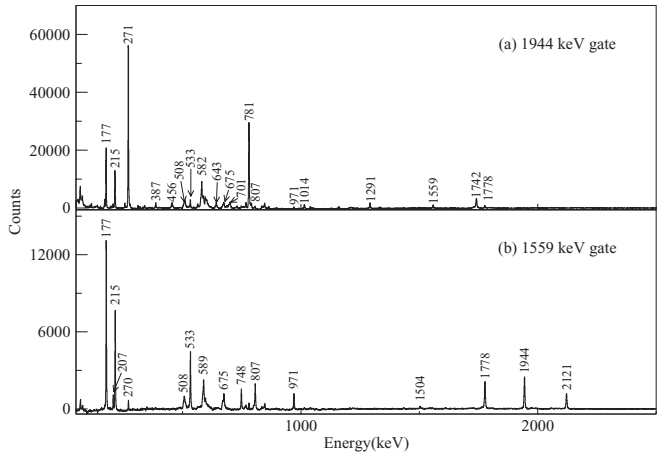

FIG. 3. (a) 1944 keV gated spectrum showing different transitions feeding to the main band, and (b) 1559 keV gated spectrum showing the different transitions connected to the negative parity states and its connection to the positive parity states.

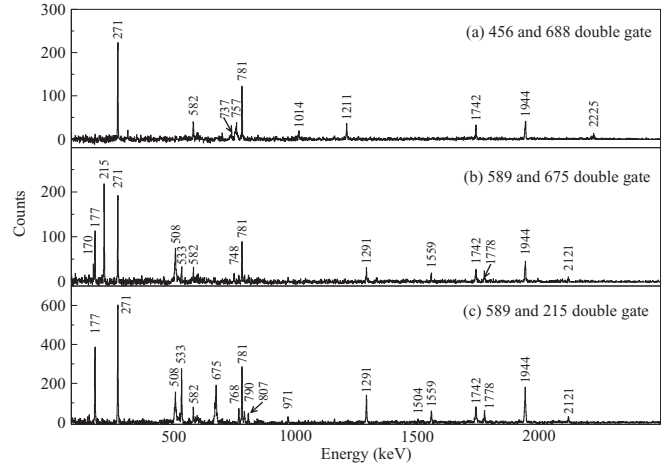

FIG. 4. Double-gated spectrum obtained by gates on (a) 456 and 688 keV, (b) 589 and 675 keV, and (c) 589 and 215 keV transitions. γ-ray transitions associated with ^{89}Zr are labeled with their energies in keV.

decaying γ transitions were determined taking into account the relative intensities, branching ratios, and the coincidence relationships between all observed γ transitions of interest.

The present level scheme consists of two parts: namely, (i) the positive parity states up to 9602 keV excitation energy, and (ii) the negative parity states up to 8016 keV excitation energy. The 1944 keV gated spectrum given in Fig. 3(a) shows the transitions, including several new transitions, feeding the $13/2^+$ state of ^{89}Zr. A number of new transitions with energies 456, 533, 643, 701, 1014, and 1291 keV decaying from the positive parity states are indicated in this spectrum. This 1944 keV gated spectrum also shows the transitions decaying from the negative parity states with energies 177, 215, 508, 675, 1559, and 1778 keV. On the other hand, the 1559 keV gated spectrum, presented in Fig. 3(b), mainly shows the different γ rays related to the negative parity states of the level scheme. The observation of several crossover and decay-out

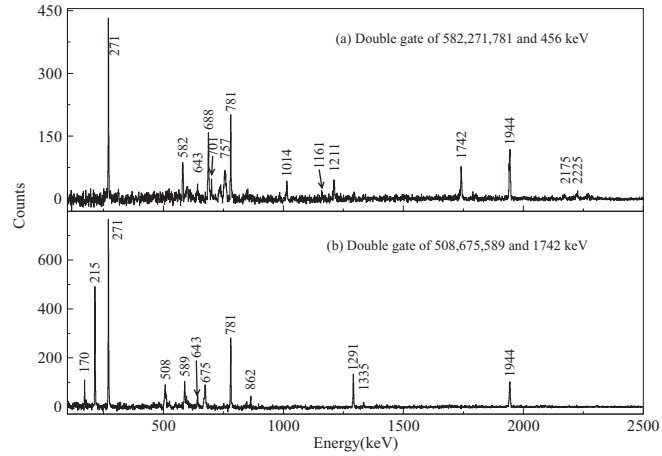

FIG. 5. Spectrum obtained by sum of the (a) double gates of 582–456, 271–456, and 781–456 keV and (b) double gates of 508–1742, 675–1742, and 589–1742 keV. γ-ray transitions associated with ^{89}Zr are labeled with their energies in keV.

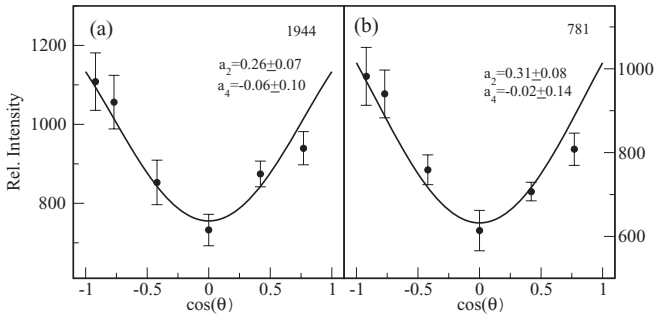

FIG. 6. Angular distribution of (a) 1944 and (b) 781 keV transitions with respect to the beam direction are plotted along with the fits and their determined multipolarities.

transitions from different levels as shown in the double gated spectra (see Figs. 4 and 5) helped in developing both positive and negative parity states. The spectra given in Figs. 4(a) and 5(a) show the various transitions of the positive parity states and their connection to the lower states. Similarly, Figs. 4(b), 4(c), and 5(b) indicate the various γ rays of the negative parity states.

One of the strongest cascades of 1944–781–271–1742–1291 keV γ rays belong to the ground band extending up to spin $I^{\pi} = 27/2^{+}$ and excitation energy of 6029 keV. The 1291 keV γ ray of this band has been newly observed in the present work, as shown in the 1944 keV gated spectrum. Two spectra generated from the sum of the double gates of 582–456, 271–456, and 781–456 keV transitions and 508–1742, 675–1742, and 589–1742 keV transitions are shown in Figs. 5(a) and 5(b), respectively. Comparison of these two spectra indicates the 582–701 keV cascade decaying from the same $I^{\pi} = 25/2^{+}$ state is feeding the $21/2^{+}$ state parallel to the 1742 keV transition. The 6029 keV state with spin $27/2^{+}$decays through other intermediate states with $23/2^{+}$ and $25/2^{+}$ spin at 3578 and 4278 keV, respectively, which is parallel to the 1742–1291 keV cascade. However, two additional $27/2^{+}$ states have also been established at excitation energies of 5382 and 5753 keV, respectively. These states are identified by the 643, 1804 and 1014, 2175 keV transitions, respectively. Three more excited $29/2^{+}$ states were also established in this part of the level scheme with excitation energies of 6110, 6354, and 6964 keV, respectively.

The 456 and 688 keV double gated spectrum given in Fig. 4(a) depicts the 757 and 737 keV γ rays feeding the $33/2^{+}$ state with energy 8108 keV. It also shows the 1014, 1211, and 2225 keV transitions connecting the $29/2^{+}$ state with an energy of 6964 keV to the lower states with positive parity. A sequence of four γ rays with energies 456, 688, 757, and 737 keV constitutes the band up to spin $(37/2^{+})$. The bandhead excitation energy is 6964 keV as it is found to decay by 1211 and 2225 keV transitions. The spin of the bandhead is confirmed by the DCO and IPDCO values of the 1014 and 1211 keV transitions. The DCO and IPDCO values of 458 and 688 keV transitions suggests firmly their $M1$ nature. However, the DCO values of the 757 and 737 keV transitions could not be extracted because of their lower intensity, and have been tentatively assigned to have $M1$ nature. Similarly, $M1$ transitions have been reported at higher excitation energies in ^{91}Mo [9].

On the negative parity side, the previously known state at 2121 keV with spin $13/2^{-}$ has been confirmed [10]. The polarization asymmetry of the 2121 keV γ ray shown in Fig. 8 shows its magnetic character. The negative parity states above the previously known state [10] with spin $17/2^{-}$ and excitation energy 3718 keV were extended up to spin $35/2^{-}$ at 8016 keV with the addition of many new transitions, including 1778, 790, 748, 589, 675, 508, and 971 keV γ rays as shown in the 1559 keV gated spectrum in Fig. 3(b). Two new transitions with energy 533 and 748 keV were found to feed the $25/2^{-}$ level at 5496 keV. The DCO and IPDCO values of the 1778 keV transition suggest negative parity for this $25/2^{-}$ state. This is further supported by a $\Delta I = 1$ $E1$ transition with energy 533 keV connecting the $25/2^{-}$ state to the $27/2^{+}$ state at 6029 keV. The excitation energy of the $29/2^{-}$ state has been fixed by the four transitions emitted from this state with energies 170, 215, 748, and 862 keV. Its spin of 29/2 has been confirmed by the DCO values of these decaying transitions, while the parity is fixed by the polarization of the 215 keV transition, which shows its electric nature (see Table I). The spin of 27/2 for the 6074 keV level has been confirmed by the DCO values of 170 and 1335 keV transitions (see Table I). Its negative parity has been assigned by the IPDCO value of 0.16(4) for the 1335 keV transition feeding the 4375 keV state with spin $25/2^{+}$.

IV. DISCUSSION AND COMPARISON WITH SHELL-MODEL CALCULATIONS

The level scheme of ^{89}Zr established in the present work indicates the persistence of shell-model-like excitations, thereby suggesting the continuation of spherical structure up to the highest observed spin. The strongly populated positive parity states up to medium spin $(27/2^{+})$ have very similar level structure to that in its nearest isotone ^{91}Mo, and suggest the contribution of seniority 1 configurations as noted in Ref. [9]. The negative parity states have been extended up to $I^{\pi} = 35/2^{-}$ along with the characteristics of single-particle excitations, as in the case of its positive parity states. However, similar low-lying negative parity states in ^{91}Mo have not been experimentally observed in the previous investigations [9], and therefore they are not available for comparison.

To interpret the experimental data for low-lying spectra and several high spin states of ^{89}Zr, state-of-the-art shell-model calculation using two different interactions have been performed. The calculations have been carried out in the 28–50 valence shell composed of the orbits $1p_{3/2}$, $0f_{5/2}$, $1p_{1/2}$, and $0g_{9/2}$, and employed two recently derived effective shell-model interactions, JUN45 and jj44b. The JUN45 interaction was recently developed by Honma *et al.* [21]. The single-particle energies employed in conjunction with the JUN45 interaction are -9.8280, -8.7087, -7.8388, and -6.2617 MeV for the $p_{3/2}$, $f_{5/2}$, $p_{1/2}$, and $g_{9/2}$ orbits, respectively. In the case of the jj44b interaction [22], the single-particle energies are -9.6566, -9.2859, -8.2695, and -5.8944 MeV for the $p_{3/2}$, $f_{5/2}$, $p_{1/2}$, and $g_{9/2}$ orbits, respectively. The calculations were performed using the shell-model code ANTOINE [34].

Figures 9 and 10 show a comparison of the experimental excitation energies of the positive and negative parity states of

TABLE I. Excitation energies of levels (E_i) in keV, γ-ray energies (E_γ) in keV, intensities, R_{DCO}, assigned multipolarities, IPDCO values, and initial and final state spins of the transitions of ^{89}Zr deduced from the present work are listed. The uncertainties in the energies of γ rays are 0.3 keV for intense peaks and 0.7 keV for weak peaks.

E_i	$J_i^\pi \rightarrow J_f^\pi$	E_γ	I_γ	R_{DCO}	IPDCO	Mult.
1944	$13/2^+ \rightarrow 9/2^+$	1944.3	100.00	0.96(1)[a]	0.13(3)	$E2$
2121	$13/2^- \rightarrow 13/2^+$	176.7	17.78(5)	0.62(2)[c]		$E1$
2121	$13/2^- \rightarrow 9/2^+$	2121.0	8.04(1)		−0.11(5)	$M2$
2151	$15/2^{(-)} \rightarrow 13/2^-$	30.0				$M1$
2151	$15/2^{(-)} \rightarrow 13/2^+$	206.7	1.13(1)	0.66(8)		$E1$
2454	$(15/2^-) \rightarrow 13/2^-$	333.0	0.70(11)			$M1$
2725	$17/2^+ \rightarrow 17/2^-$	565.0	0.15(8)	0.80(5)		$E1$
2725	$17/2^+ \rightarrow 15/2^{(-)}$	573.9	0.5(2)			$E1$
2725	$17/2^+ \rightarrow 13/2^+$	780.6	79.4(1)	1.06(1)	0.07(1)	$E2$
2928	$19/2^- \rightarrow 17/2^-$	768.1	6.14(11)	0.34(1)	−0.02(2)	$M1$
2928	$19/2^- \rightarrow 15/2^{(-)}$	777.2	0.1(5)			$E2$
2996	$21/2^+ \rightarrow 19/2^-$	67.9	0.55(10)			$E1$
2996	$21/2^+ \rightarrow 17/2^+$	271.2	69.0(3)	0.87(2)[a]	0.01(2)	$E2$
3112	$19/2^+ \rightarrow 21/2^+$	115.8	0.7(1)			$M1$
3112	$19/2^+ \rightarrow 17/2^+$	387.1	3.40(2)	0.41(1)		$M1$
3578	$23/2^+ \rightarrow 21/2^+$	581.7	22.37(4)	0.53(1)	−0.050(4)	$M1$
3718	$21/2^- \rightarrow 19/2^-$	789.8	5.30(1)	0.50(2)	−0.12(2)	$M1$
3718	$21/2^- \rightarrow 17/2^-$	1559.0	7.30(16)	1.05(4)	0.08(2)	$E2$
4278	$25/2^+ \rightarrow 23/2^+$	700.6	7.34(3)	0.44(1)		$M1$
4525	$23/2^- \rightarrow 21/2^-$	807.0	4.31(3)	0.51(2)[c]	−0.20(2)	$M1$
4739	$25/2^+ \rightarrow 25/2^+$	460.1	<0.40			$M1$
4739	$25/2^+ \rightarrow 23/2^+$	1160.7	3.59(2)	0.77(2)[d]	−0.01(1)	$M1$
4739	$25/2^+ \rightarrow 21/2^+$	1742.4	33.4(2)	0.95(4)	0.11(1)	$E2$
5382	$27/2^+ \rightarrow 25/2^+$	643.4	4.86(3)	0.41(1)	−0.10(2)	$M1$
5382	$27/2^+ \rightarrow 23/2^+$	1804.1	0.92(3)			$E2$
5496	$25/2^- \rightarrow 23/2^-$	971.0	2.17(1)	0.48(3)[c]	−0.03(5)	$M1$
5496	$25/2^- \rightarrow 21/2^-$	1778.0	5.74(5)	1.10(6)[c]	0.03(2)	$E2$
5496	$25/2^- \rightarrow 23/2^+$	1918.1	1.16(2)	0.36(4)[a]	0.03(2)	$E1$
5736	$25/2^{(+)} \rightarrow 23/2^+$	2158.1	1.09(3)			$E2$
5753	$27/2^+ \rightarrow 27/2^+$	370.9	<0.5			$M1$
5753	$27/2^+ \rightarrow 25/2^+$	1014.3	3.67(2)	0.35(1)	−0.08(1)	$M1$
5753	$27/2^+ \rightarrow 23/2^+$	2175.0	1.60(2)			$E2$
6029	$27/2^+ \rightarrow 25/2^-$	533.2	3.81(5)	0.51(2)[c]	0.10(2)	$E1$
6029	$27/2^+ \rightarrow 27/2^+$	647.2	<0.5			$M1$
6029	$27/2^+ \rightarrow 25/2^+$	1290.6	8.14(1)	0.47(1)	−0.01(1)	$M1$
6029	$27/2^+ \rightarrow 23/2^-$	1504.2	0.5(1)			$M2$
6029	$27/2^+ \rightarrow 25/2^+$	1750.7	0.53(2)			$M1$
6074	$27/2^- \rightarrow 25/2^{(+)}$	338.0	1.14(1)	1.04(9)[b]		
6074	$27/2^- \rightarrow 25/2^+$	1335.4	1.89(7)	0.43(3)[d]	0.16(4)	$E1$
6074	$27/2^- \rightarrow 25/2^+$	1795.5	0.32(1)			$E1$
6110	$(29/2^+) \rightarrow 27/2^+$	728.0	0.5(1)			$M1$
6110	$(29/2^+) \rightarrow 25/2^+$	1831.5	0.30(1)			$E2$
6244	$29/2^- \rightarrow 27/2^-$	170.0	2.10(1)	0.44(1)		$M1$
6244	$29/2^- \rightarrow 27/2^+$	214.8	10.11(4)	0.53(1)	0.02(1)	$E1$
6244	$29/2^- \rightarrow 25/2^-$	748.0	1.81(2)	1.04(8)[c]	0.08(3)	$E2$
6244	$29/2^- \rightarrow 27/2^+$	862.0	1.62(1)	0.42(2)		$E1$
6354	$(29/2^+) \rightarrow 27/2^+$	601.0	1.34(2)			$M1$
6833	$31/2^- \rightarrow 29/2^-$	589.0	6.06(32)	0.40(2)[c]	−0.08(1)	$M1$
6833	$31/2^- \rightarrow 27/2^-$	759.0	0.54(4)			$M1$
6954	$(31/2^+) \rightarrow (29/2^+)$	600.0	1.34(2)			$M1$
6964	$29/2^+ \rightarrow 27/2^+$	1211.2	3.59(12)	0.60(3)[d]	−0.09(2)	$M1$
6964	$29/2^+ \rightarrow 25/2^+$	2225.5	0.87(2)			$E2$
7420	$31/2^+ \rightarrow 29/2^+$	456.0	2.53(2)	0.49(6)	−0.03(3)	$M1$
7510	$33/2^- \rightarrow 31/2^-$	675.0	4.96(3)	0.54(8)[c]	−0.05(2)	$M1$
8018	$35/2^- \rightarrow 33/2^-$	508.0	1.81(5)	0.29(1)[d]	−0.04(1)	$M1$

TABLE I. *(Continued.)*

E_i	$J_i^\pi \rightarrow J_f^\pi$	E_γ	I_γ	R_{DCO}	IPDCO	Mult.
8108	$33/2^+ \rightarrow 31/2^+$	688.0	2.49(16)	0.44(2)[a]	−0.03(4)	$M1$
8865	$(35/2^+) \rightarrow 33/2^+$	757.0	1.57(7)			$M1$
9602	$(37/2^+) \rightarrow (35/2^+)$	737.0	1.36(8)			$M1$

R_{DCO} has been obtained with the gate indicated through the prefix of the R_{DCO} values:
[a]from the 781 keV ($E2$) DCO gate
[b]from the 582 keV ($M1$) DCO gate
[c]from the 1559 keV ($E2$) DCO gate
[d]from the 271 keV ($E2$) DCO gate
while the rest of the R_{DCO} values are obtained with 1944 keV ($E2$) gate.

^{89}Zr with the predictions of shell-model calculations obtained from the two sets of effective interactions. It is evident that the calculations have remarkably good agreement with the experimental results. In Table II, we have shown the wave functions for the ground state and the first excited state. All the interactions predict a $\nu(g_{9/2}^{-1})$ configuration for the $9/2_1^+$ ground state.

The ground state $9/2^+$ is well predicted by both interactions. The first excited $13/2^+$ state is well reproduced with an energy difference of 145 and 406 keV from JUN45 and jj44b interactions, respectively. The other calculated excitation energies for the levels with spin $I = 15/2^+, 17/2^+, 21/2^+, 19/2^+$, and $23/2^+$ have reasonable agreement with the experimental results. The only point of disagreement is the $19/2^+$ state which is observed at the excitation energy of 3112 keV and is well predicted by the JUN45 interaction, but in the case of the jj44b interaction it lies below the $21/2^+$state. The low-lying yrast states up to $25/2^+$ are well reproduced, with $\pi(f_{5/2}^{(6)} p_{3/2}^{(4)} (p_{1/2} g_{9/2})^{(2)}) \otimes \nu((p_{1/2} g_{9/2})^{(11)})$ configurations contributing maximally. The non-yrast $25/2^+$ and the three $27/2^+$ states observed in the experiment have dominant contributions from seniority 3 states involving proton excitations from $p_{3/2}$ and $f_{5/2}$ orbitals to $p_{1/2}$. The decays of these states are associated with emission of high-energy transitions with energy around 2 MeV. The experimentally observed states with energy 6964, 7420, 8108, 8865, and 9602 keV extending up to spin $37/2^+$ are well described by configurations involving proton excitations from $p_{3/2}$ and $f_{5/2}$ orbitals to $g_{9/2}$. For high spin states above $25/2^+$ to $37/2^+$ the experimental results have much better agreement with JUN45 as well as jj44b interactions.

The theoretical negative parity states have been compared to the observed states in Fig. 10. The lowest state (among the negative parity states) observed in the present experiment is $13/2^-$ with energy 2121 keV. For this $13/2^-$ state, the difference between experiment and theory is 174 and 93 keV for JUN45 and jj44b interactions, respectively. The state has a dominant contribution from the $\pi(f_{5/2}^{(6)} p_{3/2}^{(4)} p_{1/2}^{(1)} g_{9/2}^{(1)}) \otimes \nu((p_{1/2} g_{9/2})^{(11)})$ configuration. The same configuration continues to dominate up to $19/2^-$. From $21/2^-$ onward up to $35/2^-$ the states have dominant contributions from proton excitation from the $f_{5/2}$ orbital to $g_{9/2}$, and are quite well explained by the shell-model calculations.

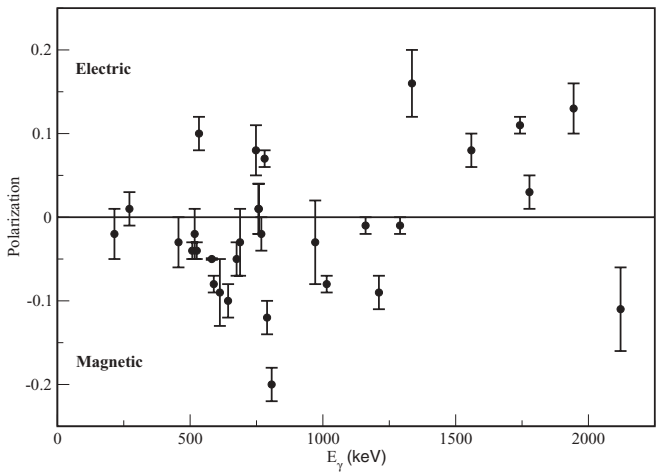

FIG. 7. Plot for polarization asymmetry for different transitions.

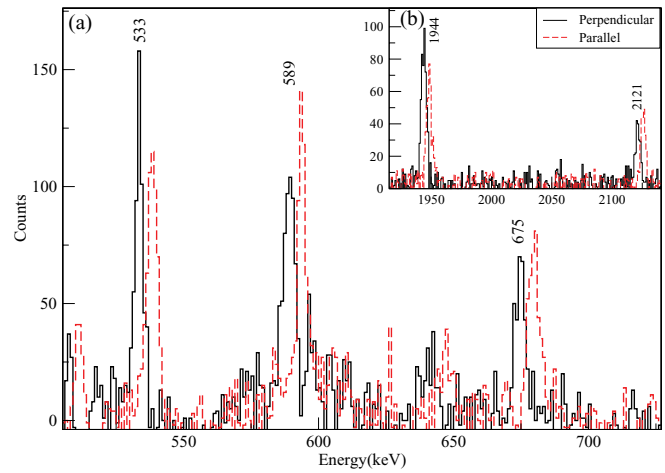

FIG. 8. (Color online) 1559 keV gated spectrum of the perpendicular and parallel Compton scattering in the 90° clover detectors. The parallel scattering spectrum has been shifted by 4 keV for better visualization. Higher counts for 589 and 675 keV transitions in the parallel scattered spectrum indicates their magnetic character while the reverse condition suggests the electric nature for the 533 keV transition. The inset spectrum confirms the electric and magnetic nature for the previously known 1944 and 2121 keV transitions, respectively.

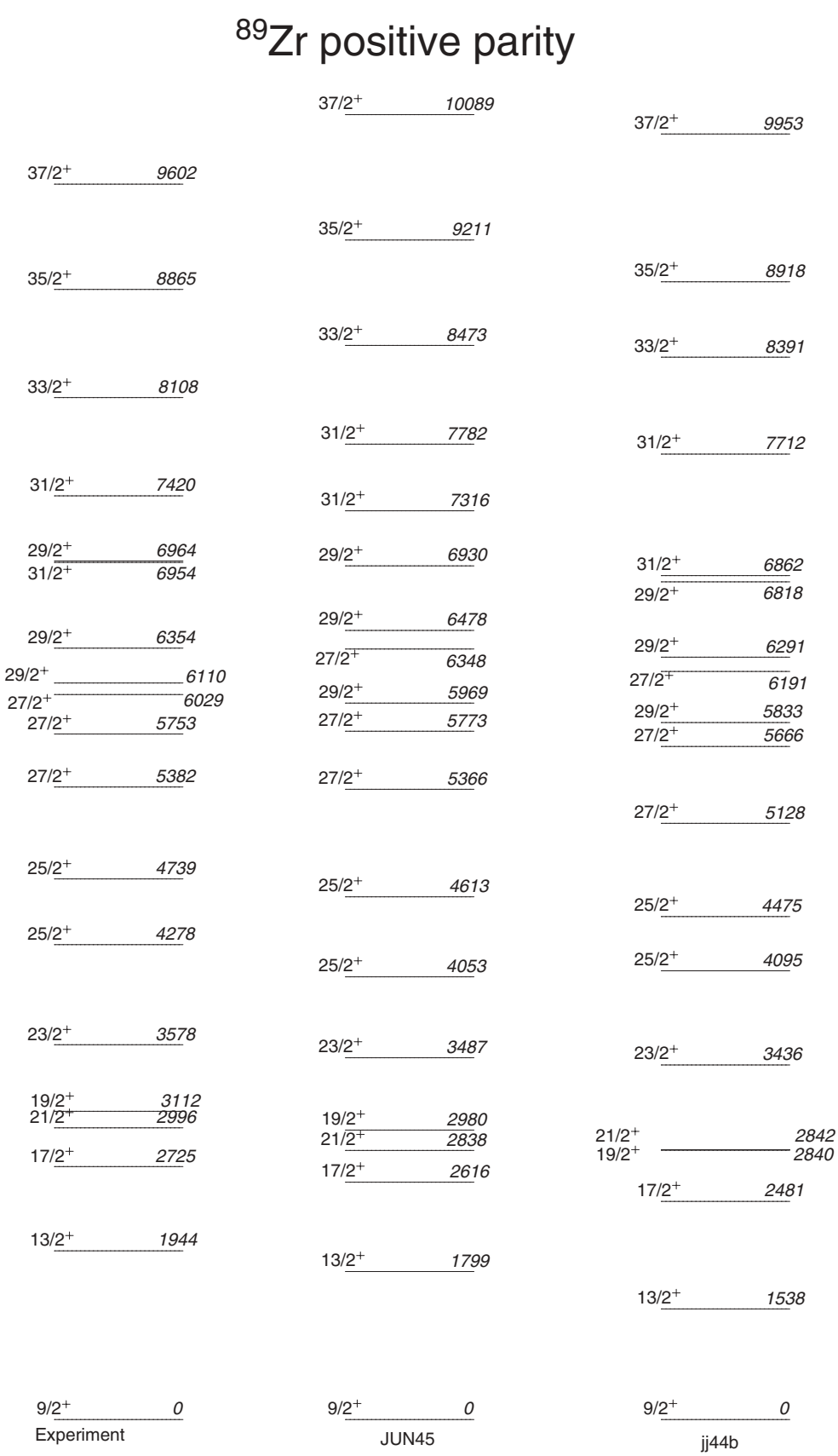

FIG. 9. Calculated and experimental level schemes consisting of the positive parity states of ^{89}Zr, with two different interactions for calculations.

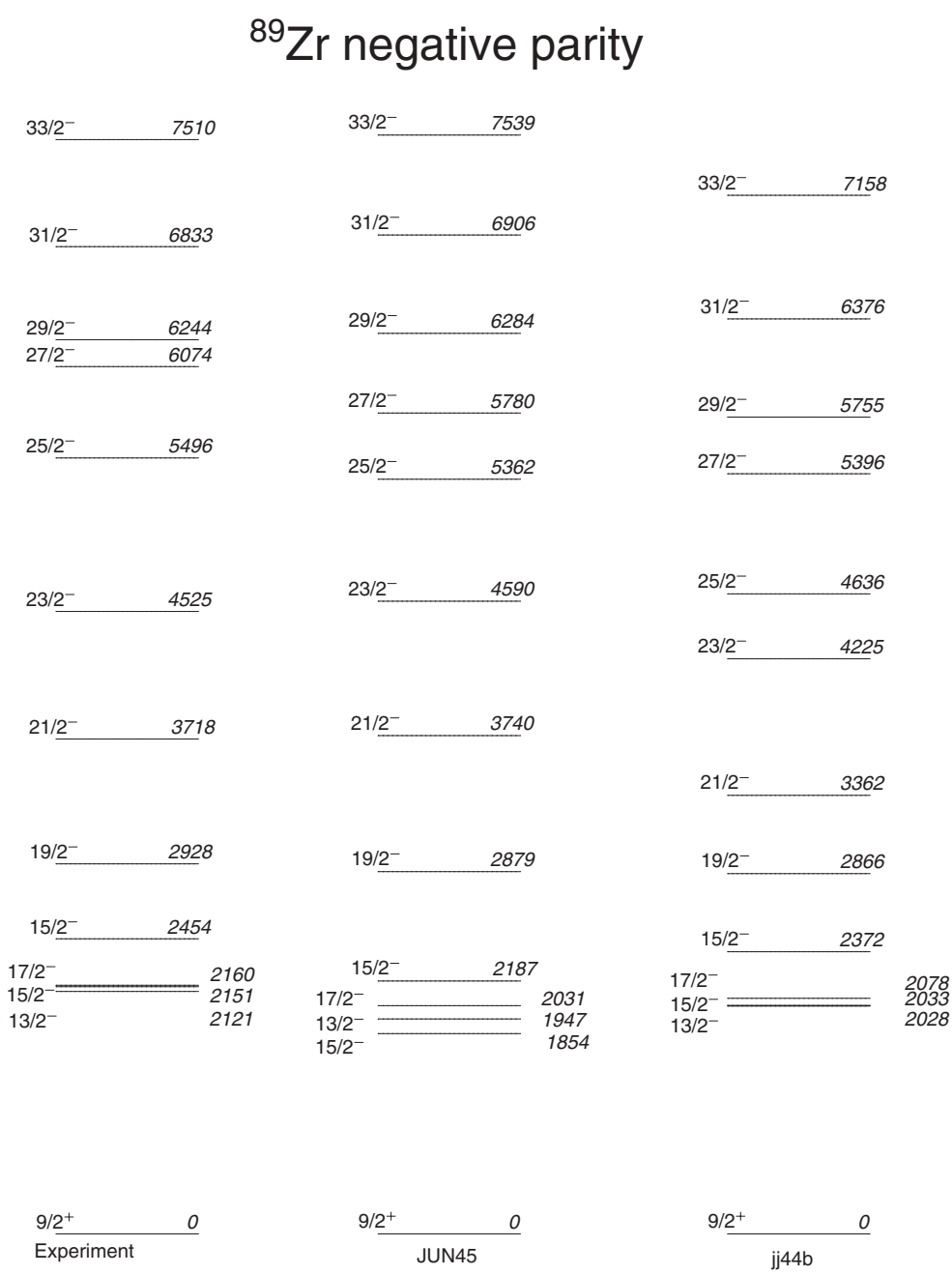

FIG. 10. Calculated and experimental level schemes consisting of the negative parity states of ^{89}Zr, with two different interactions for calculation.

In general, the calculations performed with these set of effective interactions significantly improve the predictive power of calculations and are in good agreement with experimental data up to very high spin positive parity states. The experimentally observed highest spin state with $J^\pi = 37/2^+$ with an energy of 9602 keV is reproduced in the calculation within 460 and 343 keV differences in JUN45 and jj44b interactions, respectively. The calculated energy levels for the negative parity states up to $J^\pi = 17/2^-$ from the jj44b interaction is closer to the experimental results compared to the JUN45 interaction. Also the ordering of the energy levels with increasing spin values obtained with jj44b matches with the measured negative parity states at lower spin. On the other hand, the JUN45 interaction predicts the lowest $15/2^-$ state to be lower compared to the lowest $13/2^-$ state, in contradiction with the level scheme established in the present work. However, for the high spin states in the negative parity band the agreement of the results of JUN45 with the experiment is better than that of jj44b. The results of the JUN45 interaction are surprisingly close to the measured states, with less than 100 keV difference for states from $J^\pi = 19/2^-$ onward.

TABLE II. Wave functions for the ^{89}Zr for ground state and a few excited states.

I	Probability	JUN45 Wave functions		Probability	jj44b Wave functions	
		Proton	Neutron		Proton	Neutron
$9/2^+_{g.s.}$	36.4%	$p^4_{3/2}f^6_{5/2}p^2_{1/2}g^0_{9/2}$	$p^4_{3/2}f^6_{5/2}p^2_{1/2}g^9_{9/2}$	22.0%	$p^4_{3/2}f^6_{5/2}p^2_{1/2}g^0_{9/2}$	$p^4_{3/2}f^6_{5/2}p^2_{1/2}g^9_{9/2}$
$13/2^+_1$	48.8%	$p^4_{3/2}f^6_{5/2}p^0_{1/2}g^2_{9/2}$	$p^4_{3/2}f^6_{5/2}p^2_{1/2}g^9_{9/2}$	33.0%	$p^4_{3/2}f^6_{5/2}p^0_{1/2}g^2_{9/2}$	$p^4_{3/2}f^6_{5/2}p^2_{1/2}g^9_{9/2}$
$15/2^+_1$	56.1%	$p^4_{3/2}f^6_{5/2}p^0_{1/2}g^2_{9/2}$	$p^4_{3/2}f^6_{5/2}p^2_{1/2}g^9_{9/2}$	40.4%	$p^4_{3/2}f^6_{5/2}p^0_{1/2}g^2_{9/2}$	$p^4_{3/2}f^6_{5/2}p^2_{1/2}g^9_{9/2}$
$17/2^+_1$	54.8%	$p^4_{3/2}f^6_{5/2}p^0_{1/2}g^2_{9/2}$	$p^4_{3/2}f^6_{5/2}p^2_{1/2}g^9_{9/2}$	40.9%	$p^4_{3/2}f^6_{5/2}p^0_{1/2}g^2_{9/2}$	$p^4_{3/2}f^6_{5/2}p^2_{1/2}g^9_{9/2}$
$19/1^+_1$	55.7%	$p^4_{3/2}f^6_{5/2}p^0_{1/2}g^2_{9/2}$	$p^4_{3/2}f^6_{5/2}p^2_{1/2}g^9_{9/2}$	40.1%	$p^4_{3/2}f^6_{5/2}p^0_{1/2}g^2_{9/2}$	$p^4_{3/2}f^6_{5/2}p^2_{1/2}g^9_{9/2}$
$21/2^+_1$	56.8%	$p^4_{3/2}f^6_{5/2}p^0_{1/2}g^2_{9/2}$	$p^4_{3/2}f^6_{5/2}p^2_{1/2}g^9_{9/2}$	43.6%	$p^4_{3/2}f^6_{5/2}p^0_{1/2}g^2_{9/2}$	$p^4_{3/2}f^6_{5/2}p^2_{1/2}g^9_{9/2}$
$23/2^+_1$	56.5%	$p^4_{3/2}f^6_{5/2}p^0_{1/2}g^2_{9/2}$	$p^4_{3/2}f^6_{5/2}p^2_{1/2}g^9_{9/2}$	43.3%	$p^4_{3/2}f^6_{5/2}p^0_{1/2}g^2_{9/2}$	$p^4_{3/2}f^6_{5/2}p^2_{1/2}g^9_{9/2}$
$25/2^+_1$	56.8%	$p^4_{3/2}f^6_{5/2}p^0_{1/2}g^2_{9/2}$	$p^4_{3/2}f^6_{5/2}p^2_{1/2}g^9_{9/2}$	45.3%	$p^4_{3/2}f^6_{5/2}p^0_{1/2}g^2_{9/2}$	$p^4_{3/2}f^6_{5/2}p^2_{1/2}g^9_{9/2}$
$25/2^+_2$	36.4%	$p^4_{3/2}f^5_{5/2}p^1_{1/2}g^2_{9/2}$	$p^4_{3/2}f^6_{5/2}p^2_{1/2}g^9_{9/2}$	53.0%	$p^4_{3/2}f^5_{5/2}p^1_{1/2}g^2_{9/2}$	$p^4_{3/2}f^6_{5/2}p^2_{1/2}g^9_{9/2}$
$27/2^+_1$	35.3%	$p^4_{3/2}f^5_{5/2}p^1_{1/2}g^2_{9/2}$	$p^4_{3/2}f^6_{5/2}p^2_{1/2}g^9_{9/2}$	59.2%	$p^4_{3/2}f^5_{5/2}p^1_{1/2}g^2_{9/2}$	$p^4_{3/2}f^6_{5/2}p^2_{1/2}g^9_{9/2}$
$27/2^+_2$	60.7%	$p^4_{3/2}f^5_{5/2}p^1_{1/2}g^2_{9/2}$	$p^4_{3/2}f^6_{5/2}p^2_{1/2}g^9_{9/2}$	54.5%	$p^4_{3/2}f^5_{5/2}p^1_{1/2}g^2_{9/2}$	$p^4_{3/2}f^6_{5/2}p^2_{1/2}g^9_{9/2}$
$27/2^+_3$	38.8%	$p^3_{3/2}f^5_{5/2}p^2_{1/2}g^2_{9/2}$	$p^4_{3/2}f^6_{5/2}p^2_{1/2}g^9_{9/2}$	63.5%	$p^4_{3/2}f^5_{5/2}p^1_{1/2}g^2_{9/2}$	$p^4_{3/2}f^6_{5/2}p^2_{1/2}g^9_{9/2}$
$29/2^+_1$	34.1%	$p^3_{3/2}f^6_{5/2}p^1_{1/2}g^2_{9/2}$	$p^4_{3/2}f^6_{5/2}p^2_{1/2}g^9_{9/2}$	56.8%	$p^4_{3/2}f^5_{5/2}p^1_{1/2}g^2_{9/2}$	$p^4_{3/2}f^6_{5/2}p^2_{1/2}g^9_{9/2}$
$29/2^+_2$	65.8%	$p^4_{3/2}f^5_{5/2}p^1_{1/2}g^2_{9/2}$	$p^4_{3/2}f^6_{5/2}p^2_{1/2}g^9_{9/2}$	53.6%	$p^4_{3/2}f^5_{5/2}p^1_{1/2}g^2_{9/2}$	$p^4_{3/2}f^6_{5/2}p^2_{1/2}g^9_{9/2}$
$29/2^+_3$	43.5%	$p^3_{3/2}f^5_{5/2}p^2_{1/2}g^2_{9/2}$	$p^4_{3/2}f^6_{5/2}p^2_{1/2}g^9_{9/2}$	26.0%	$p^3_{3/2}f^5_{5/2}p^0_{1/2}g^4_{9/2}$	$p^4_{3/2}f^6_{5/2}p^2_{1/2}g^9_{9/2}$
$31/2^+_1$	74.6%	$p^4_{3/2}f^5_{5/2}p^1_{1/2}g^2_{9/2}$	$p^4_{3/2}f^6_{5/2}p^2_{1/2}g^9_{9/2}$	73.2%	$p^4_{3/2}f^5_{5/2}p^1_{1/2}g^2_{9/2}$	$p^4_{3/2}f^6_{5/2}p^2_{1/2}g^9_{9/2}$
$31/2^+_2$	42.5%	$p^3_{3/2}f^5_{5/2}p^2_{1/2}g^2_{9/2}$	$p^4_{3/2}f^6_{5/2}p^2_{1/2}g^9_{9/2}$	33.7%	$p^3_{3/2}f^5_{5/2}p^0_{1/2}g^4_{9/2}$	$p^4_{3/2}f^6_{5/2}p^2_{1/2}g^9_{9/2}$
$33/2^+_1$	32.6%	$p^3_{3/2}f^5_{5/2}p^0_{1/2}g^4_{9/2}$	$p^4_{3/2}f^6_{5/2}p^2_{1/2}g^9_{9/2}$	29.6%	$p^4_{3/2}f^4_{5/2}p^0_{1/2}g^4_{9/2}$	$p^4_{3/2}f^6_{5/2}p^2_{1/2}g^9_{9/2}$
$35/2^+_1$	68.7%	$p^3_{3/2}f^5_{5/2}p^0_{1/2}g^4_{9/2}$	$p^4_{3/2}f^6_{5/2}p^2_{1/2}g^9_{9/2}$	61.5%	$p^3_{3/2}f^5_{5/2}p^0_{1/2}g^4_{9/2}$	$p^4_{3/2}f^6_{5/2}p^2_{1/2}g^9_{9/2}$
$37/2^+_1$	60.1%	$p^3_{3/2}f^5_{5/2}p^0_{1/2}g^4_{9/2}$	$p^4_{3/2}f^6_{5/2}p^2_{1/2}g^9_{9/2}$	48.1%	$p^4_{3/2}f^4_{5/2}p^0_{1/2}g^4_{9/2}$	$p^4_{3/2}f^6_{5/2}p^2_{1/2}g^9_{9/2}$
$13/2^-_1$	64.1%	$p^4_{3/2}f^6_{5/2}p^1_{1/2}g^1_{9/2}$	$p^4_{3/2}f^6_{5/2}p^2_{1/2}g^9_{9/2}$	45.0%	$p^4_{3/2}f^6_{5/2}p^1_{1/2}g^1_{9/2}$	$p^4_{3/2}f^6_{5/2}p^2_{1/2}g^9_{9/2}$
$15/2^-_1$	60.2%	$p^4_{3/2}f^6_{5/2}p^1_{1/2}g^1_{9/2}$	$p^4_{3/2}f^6_{5/2}p^2_{1/2}g^9_{9/2}$	48.1%	$p^4_{3/2}f^6_{5/2}p^1_{1/2}g^1_{9/2}$	$p^4_{3/2}f^6_{5/2}p^2_{1/2}g^9_{9/2}$
$15/2^-_2$	66.4%	$p^4_{3/2}f^6_{5/2}p^1_{1/2}g^1_{9/2}$	$p^4_{3/2}f^6_{5/2}p^2_{1/2}g^9_{9/2}$	48.7%	$p^4_{3/2}f^6_{5/2}p^0_{1/2}g^2_{9/2}$	$p^4_{3/2}f^6_{5/2}p^2_{1/2}g^9_{9/2}$
$17/2^-_1$	66.7%	$p^4_{3/2}f^6_{5/2}p^1_{1/2}g^1_{9/2}$	$p^4_{3/2}f^6_{5/2}p^2_{1/2}g^9_{9/2}$	52.9%	$p^4_{3/2}f^6_{5/2}p^1_{1/2}g^1_{9/2}$	$p^4_{3/2}f^6_{5/2}p^2_{1/2}g^9_{9/2}$
$19/2^-_1$	68.0%	$p^4_{3/2}f^6_{5/2}p^1_{1/2}g^1_{9/2}$	$p^4_{3/2}f^6_{5/2}p^2_{1/2}g^9_{9/2}$	52.5%	$p^4_{3/2}f^6_{5/2}p^1_{1/2}g^1_{9/2}$	$p^4_{3/2}f^6_{5/2}p^2_{1/2}g^9_{9/2}$
$21/2^-_1$	40.5%	$p^4_{3/2}f^5_{5/2}p^2_{1/2}g^1_{9/2}$	$p^4_{3/2}f^6_{5/2}p^2_{1/2}g^9_{9/2}$	31.6%	$p^4_{3/2}f^5_{5/2}p^0_{1/2}g^3_{9/2}$	$p^4_{3/2}f^6_{5/2}p^2_{1/2}g^9_{9/2}$
$23/2^-_1$	37.3%	$p^4_{3/2}f^5_{5/2}p^2_{1/2}g^1_{9/2}$	$p^4_{3/2}f^6_{5/2}p^2_{1/2}g^9_{9/2}$	35.9%	$p^4_{3/2}f^5_{5/2}p^0_{1/2}g^3_{9/2}$	$p^4_{3/2}f^6_{5/2}p^2_{1/2}g^9_{9/2}$
$25/2^-_1$	61.6%	$p^4_{3/2}f^5_{5/2}p^0_{1/2}g^3_{9/2}$	$p^4_{3/2}f^6_{5/2}p^2_{1/2}g^9_{9/2}$	52.9%	$p^4_{3/2}f^5_{5/2}p^0_{1/2}g^3_{9/2}$	$p^4_{3/2}f^6_{5/2}p^2_{1/2}g^9_{9/2}$
$27/2^-_1$	68.9%	$p^3_{3/2}f^6_{5/2}p^0_{1/2}g^3_{9/2}$	$p^4_{3/2}f^6_{5/2}p^2_{1/2}g^9_{9/2}$	49.8%	$p^4_{3/2}f^5_{5/2}p^0_{1/2}g^3_{9/2}$	$p^4_{3/2}f^6_{5/2}p^2_{1/2}g^9_{9/2}$
$29/2^-_1$	64.4%	$p^4_{3/2}f^5_{5/2}p^0_{1/2}g^3_{9/2}$	$p^4_{3/2}f^6_{5/2}p^2_{1/2}g^9_{9/2}$	55.3%	$p^4_{3/2}f^5_{5/2}p^0_{1/2}g^3_{9/2}$	$p^4_{3/2}f^6_{5/2}p^2_{1/2}g^9_{9/2}$
$31/2^-_1$	63.9%	$p^4_{3/2}f^5_{5/2}p^0_{1/2}g^3_{9/2}$	$p^4_{3/2}f^6_{5/2}p^2_{1/2}g^9_{9/2}$	56.2%	$p^4_{3/2}f^5_{5/2}p^0_{1/2}g^3_{9/2}$	$p^4_{3/2}f^6_{5/2}p^2_{1/2}g^9_{9/2}$
$33/2^-_1$	63.1%	$p^4_{3/2}f^5_{5/2}p^0_{1/2}g^3_{9/2}$	$p^4_{3/2}f^6_{5/2}p^2_{1/2}g^9_{9/2}$	56.4%	$p^4_{3/2}f^5_{5/2}p^0_{1/2}g^3_{9/2}$	$p^4_{3/2}f^6_{5/2}p^2_{1/2}g^9_{9/2}$

V. SUMMARY AND CONCLUSIONS

The previously known level scheme of ^{89}Zr has been substantially extended with the addition of around 35 new transitions in a measurement using the $^{13}C + ^{80}Se$ reaction at 50 MeV beam energy. The spin and parity of different states up to spin of $37/2\,\hbar$ and excitation energy of $\sim$10 MeV have been established through angular correlation and polarization measurements. The low-lying positive parity states in ^{89}Zr show remarkable similarity with that of the nearby $N = 49$ isotones. Both the positive as well as the negative parity states up to highest observed excitation energy and spins indicate the dominance of single-particle excitations in this nucleus. Therefore, the high spin states in this ^{89}Zr provided a testing ground of the predictions of the shell-model calculations with different residual interactions. The observed states are compared with state-of-the-art shell-model calculations in the 28–50 valence space. Though the results of JUN45 and jj44b interactions for the f_5pg_9 shell space show overall good agreement with experimental data, there is scope for improvements of the calculations to understand their observed discrepancies with the measurements. The shell-model calculations indicate the important role played by interactions between the excitation of the valence protons outside the $Z = 40$ subshell. On the experimental side, more measurements are required to explore the higher spin states to investigate neutron excitations across the $N = 50$ shell gap, as well

as the possible emergence of collective excitations through reactions more symmetrical than the one used in the present work.

ACKNOWLEDGMENTS

Authors would like to thank the TIFR-BARC Pelletron Linac Facility staff for providing good quality beams. The help and cooperation of the members of the INGA collaboration in setting up the array is acknowledged. This work was partially funded by the Department of Science and Technology, Government of India (No. IR/S2/PF-03/2003-I). The shell-model calculations have been performed at the KanBalam computational facility of DGCTIC-UNAM. P.C.S. acknowledges support in part by Conacyt, México, and by DGAPA, UNAM Project No. IN103212. U.G. gratefully acknowledges the hospitality of TIFR, Mumbai.

[1] S. E. Arnell, D. Foltescu, H. A. Roth, Ö. Skeppstedt, J. Blomqvist, A. Nilsson, T. Kuroyanagi, S. Mitarai, and J. Nyberg, Phys. Rev. C **49**, 51 (1994).
[2] D. Rudolph, K. P. Lieb, and H. Grawe, Nucl. Phys. A **597**, 298 (1996).
[3] H. Herndl and B. A. Brown, Nucl. Phys. A **627**, 35 (1997).
[4] T. Fukuchi *et al*., Eur. Phys. J. A **24**, 249 (2005).
[5] N. Yoshinaga, K. Higashiyama, and P. H. Regan, Phys. Rev. C **78**, 044320 (2008).
[6] A. V. Afanasjev and I. Ragnarsson, Nucl. Phys. A **586**, 377 (1995).
[7] N. Fotiades *et al*., Phys. Rev. C **74**, 034308 (2006).
[8] Pragya Singh, R. G. Pillay, J. A. Sheikh, and H. G. Devare, Phys. Rev. C **48**, 1609 (1993).
[9] S. Ray, N. S. Pattabiraman, R. Goswami, S. S. Ghugre, A. K. Sinha, and U. Garg, Phys. Rev. C **69**, 054314 (2004).
[10] E. K. Warburton, J. W. Olness, C. J. Lister, J. A. Becker, and S. D. Bloom, J. Phys. G **12**, 1017 (1986).
[11] A. Nilsson and M. Grecescu, Nucl. Phys. A **212**, 448 (1973).
[12] P. Guazzoni *et al*., Nucl. Phys. A **697**, 611 (2002).
[13] H. J. Kim and R. L. Robinson, Phys. Rev. **162**, 1036 (1967).
[14] M. S. Greenwood, M. Pluta, N. Anantaraman, and L. R. Greenwood, Phys. Rev. C **11**, 1995 (1975).
[15] G. Duhamel-Chretien, G. Perrin, C. Perrin, V. Comparat, E. Gerlic, S. Gales, and C. P. Massolo, Phys. Rev. C **43**, 1116 (1991).
[16] E. L. Robinson, R. C. Hagenauer, and E. Eichler, Nucl. Phys. A **123**, 471 (1969).
[17] D. H. Gloeckner and F. J. D. Serduke, Nucl. Phys. A **220**, 477 (1974).
[18] F. J. D. Serduke, R. D. Lawson, and D. H. Gloeckner, Nucl. Phys. A **256**, 45 (1976).
[19] S. S. Ghugre and S. K. Datta, Phys. Rev. C **52**, 1881 (1995).
[20] I. P. Johnstone and L. D. Skouras, Eur. Phys. J. A **11**, 125 (2001).
[21] M. Honma, T. Otsuka, T. Mizusaki, and M. Hjorth-Jensen, Phys. Rev. C **80**, 064323 (2009).
[22] B. A. Brown and A. F. Lisetskiy (unpublished).
[23] B. Cheal *et al*., Phys. Rev. Lett. **104**, 252502 (2010).
[24] G. J. Kumbartzki *et al*., Phys. Rev. C **85**, 044322 (2012).
[25] R. Palit, in *Application of Accelerators in Research and Industry: Twenty-First International Conference*, edited by F. D. McDaniel and B. L. Doyle, AIP Conf. Proc. No. 1336 (AIP, New York, 2011), p. 573.
[26] H. Tan *et al*., in *2008 IEEE Nuclear Science Symposium and Medical Imaging Conference (2008 NSS/MIC)*, Dresdan, 2008 (IEEE, New York, 2009), p. 2471.
[27] R. Palit *et al*., Nucl. Instrum. Methods A **680**, 90 (2012).
[28] M. Saha Sarkar *et al*. (private communication).
[29] D. C. Radford, Nucl. Instrum. Methods A **361**, 297 (1995).
[30] A. Krämer-Flecken, T. Morek, R. M. Lieder, W. Gast, G. Hebbinghaus, H. M. Jäger, and W. Urban, Nucl. Instrum. Methods A **275**, 333 (1989).
[31] K. Starosta *et al*., Nucl. Instrum. Methods A **423**, 16 (1999).
[32] R. Palit, H. C. Jain, P. K. Joshi, S. Nagaraj, B. V. T. Rao, S. N. Chintalapudi, and S. S. Ghugre, Pramana **54**, 347 (2000).
[33] S. Lakshmi, H. C. Jain, P. K. Joshi, I. Mazumdar, R. Palit, A. K. Jain, and S. S. Malik, Nucl. Phys. A **761**, 1 (2005).
[34] E. Caurier, G. Martínez-Pinedo, F. Nowacki, A. Poves, and A. P. Zuker, Rev. Mod. Phys. **77**, 427 (2005).